Research Article

Genetically engineered human embryonic kidney cells as a novel vehicle for dual patch clamp study of human gap junction channels

Honghong Chen[1], Yi X. Li[1], Robert S. Wong[1], Jessica L. Esseltine[2] and ⓘDonglin Bai[1]

[1]Department of Physiology and Pharmacology, University of Western Ontario, London, Ontario, Canada N6A 5C1; [2]Division of BioMedical Sciences, Faculty of Medicine, Memorial University of Newfoundland, St. John's, Newfoundland and Labrador, Canada A1B 3V6

Correspondence: Donglin Bai (donglin.bai@schulich.uwo.ca)

Mutations in more than half of human connexin genes encoding gap junction (GJ) subunits have been linked to inherited human diseases. Functional studies of human GJ channels are essential for revealing mechanistic insights into the etiology of disease-linked connexin mutants. However, the commonly used *Xenopus* oocytes, N2A, HeLa, and other model cells for recombinant expression of human connexins have different and significant limitations. Here we developed a human cell line (HEK293) with each of the endogenous connexins (Cx43 and Cx45) knocked out using the CRISPR-Cas9 system. Double knockout HEK293 cells showed no background GJ coupling, were easily transfected with several human connexin genes (such as those encoding Cx46, Cx50, Cx37, Cx45, Cx26, and Cx36) which successfully formed functional GJs and were readily accessible for dual patch clamp analysis. Single knockout Cx43 or Cx45 HEK cell lines could also be used to characterize human GJ channels formed by Cx45 or Cx43, respectively, with an expression level suitable for studying macroscopic and single channel GJ channel properties. A cardiac arrhythmia linked Cx45 mutant R184G failed to form functional GJs in DKO HEK293 cells with impaired localizations. These genetically engineered HEK293 cells are well suited for patch clamp study of human GJ channels.

Introduction

Gap junction (GJ) channels are ubiquitous in our body mediating direct intercellular communications in various tissues and organs [1,2]. A GJ channel is composed of two head-to-head docked hemichannels and each hemichannel is a hexamer of connexins [2]. Twenty-one connexin genes are in the human genome encoding different connexins with distinct tissue distribution [3,4]. Each tissue cell often expresses more than one type of connexin to form various types of GJ channels to meet the demand of intercellular communication in different tissues and organs [1,5]. The biological importance of GJ channels is best demonstrated by the fact that numerous mutations in more than half of connexin genes have been linked to inherited diseases, including sensorineural hearing loss, hypomyelination diseases, cataracts, cardiac arrhythmias, and developmental disease [6–8]. To establish if these disease-linked connexin variants play a pathogenic role in patients carrying connexin variant genes, one would need to have evidence of functional impairment associated with these variants. However, most of the functional studies on human disease-linked connexin mutants are conducted on non-mammalian *Xenopus* oocyte expression systems, rodent cell lines, such as mouse neuroblastoma cells (N2A), and/or a human cervical cancer cell lines, HeLa cells [9–14]. In these expression systems, human connexins were mostly expressed well and were able to assemble into functional hemichannels and/or GJ channels for functional characterization. However, each of these commonly used expression systems showed some important limitations.

Xenopus oocytes are excellent cells for recombinant expression of connexins/innexins from vertebrates and invertebrates for their GJ and/or hemichannel studies [15–17]. The large size of the oocytes and their nuclei made it possible to inject mRNA or cDNA encoding for connexin genes and study the resultant GJ or hemichannel properties with two-electrode voltage clamp technique [18,19]. This approach is still used by several laboratories to study GJ and/or hemichannels [9,13,20]. But here are some limitations for functional studies of GJ channels using *Xenopus* oocytes: (1) they are non-mammalian cells with different posttranslational modifications from those in the mammalian cells, such as, phosphorylation, glycosylation, ubiquitination, etc. [21–23]; (2) to study GJ functions in oocyte pairs requires dedicated specialized two-electrode voltage clamp systems to perform voltage clamp [18,19]; (3) endogenously expressed Cx38 could form functional GJs or mix with expressed connexins to form various types of GJs, complicating data analysis and interpretations [16,24]. This was a big issue in early studies prior to the use of antisense RNA against Cx38; (4) the number of GJ channels formed between oocyte pairs is very high and therefore this approach cannot be used for single GJ channel studies.

Mouse neuroblastoma (N2A) cells are mammalian cells with many posttranslational modifications closely resemble to those in human cells and they are well suited to study both macroscopic and single GJ channel currents with dual patch clamp technique [25–27]. N2A cells are connexin-deficient, susceptible to transfection of connexin genes, and their sphere shape makes them the best choice for patch clamp study of human GJs. Though most human connexins are expressed well in N2A cells and able to form functional GJs [28–30], human Cx46 has been shown to be extremely difficult to express in this mouse cell line [11,31]. Researchers frequently use rodent version of Cx46 to study their GJ function [32,33]. The reason for human Cx46 not expressing well in N2A cells is not clear but may be related to the fact that this is a mouse cell line and may not represent the cellular context of human cells [26].

Human cervical cancer cell line, HeLa cell, is another commonly used model cell for GJ studies [34,35]. Like those found in N2A cells, HeLa cells are also connexin deficient and susceptible to transfection of connexin genes or generating stable connexin expression lines. But their flat morphology is not a friendly feature for patch clamp study for GJ or hemichannels. This feature, however, is more suitable for morphological studies on GJ localizations [10,30,32]. In addition, HeLa cells are also frequently used for dye transfer through GJ channels or dye upload via connexin hemichannels or other large pore channels [36,37]. One of the biggest limitations of using HeLa cells for functional study of GJ channels is its high genetic instability [38], which could change their morphology and, in some cases, turn on expression of connexins to form background GJ coupling contaminating the expressed GJ channels [39].

There are other less commonly used expression model cells, such as (1) human hepatoma SKHep1 cell line [40], which showed a relatively high (~15%) background GJ coupling in cell pairs [41]; (2) rat insulinoma (RIN) cells were connexin deficient and were used for expression study of connexins [42–44] to study GJ properties and cell cycles. As RIN cells are rat cell line, it is not clear if all human connexins could express well and form functional GJs in this expression system. Even if they were expressed, they would still be in the cell context of a rodent cell line.

The limitations of these recombinant expression systems call for a novel improved *in vitro* model cell system to study human connexins, ideally in a human cellular context. Here we developed genetically engineered human embryonic kidney (HEK293) cells to eliminate endogenous connexins, by knocking out both Cx43 and Cx45 using CRISPR-Cas9. Double knockout HEK293 cells showed no GJ coupling for multiple passages, and were susceptible to transfection of human connexin genes, including Cx46, to form functional GJ channels. Importantly, these cells were easily accessible for dual patch clamp analysis for functional study of disease-linked connexin variants. We also characterized GJ channel properties in single Cx43 or Cx45 knockout cells and confirmed that the GJs in these single knockout lines are formed by Cx45 or Cx43, respectively. The endogenously expressed Cx43 or Cx45 were expressed at a suitable level to study either macroscopic or single GJ channels. Taken together, genetically engineered HEK293 cells are excellent model cells for studying human GJ channels.

Results

Endogenous GJ coupling in HEK293 cells was eliminated in the cells with both Cx43 and Cx45 genes knocked out

To study endogenous GJ coupling in HEK293 cells, we selected isolated cell pairs to perform dual whole cell voltage clamp to measure transjunctional currents (I_js) in response to a transjunctional voltage ($V_j = -20$ mV). As shown in Figure 1, representative I_js were recorded from WT, Cx45 knockout (Cx45KO), Cx43 knockout
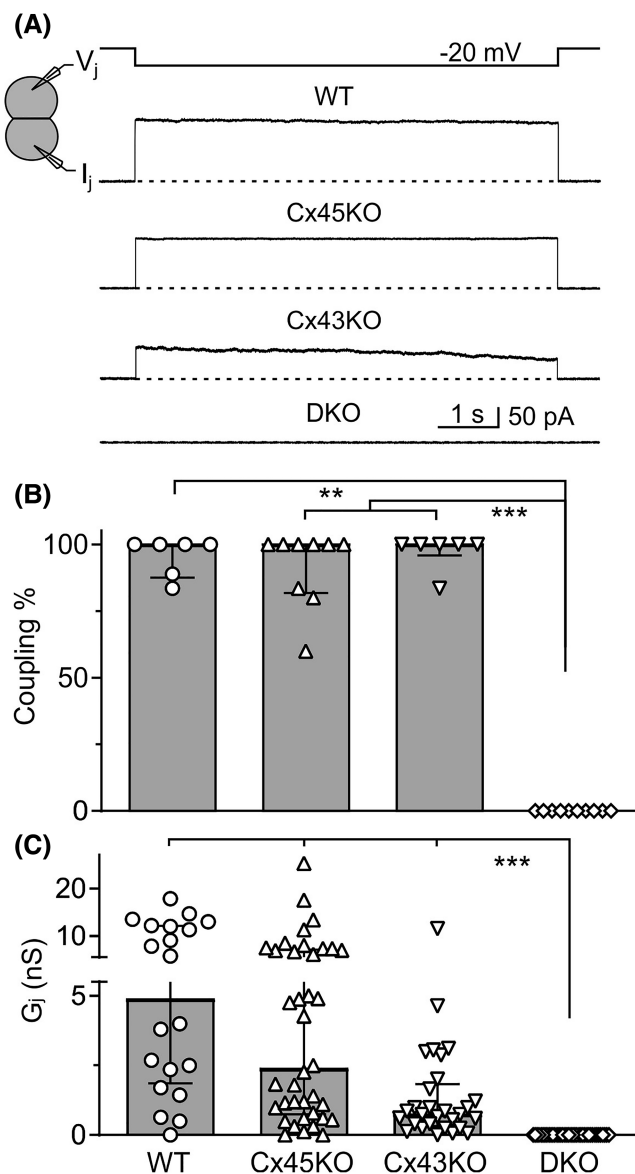
Figure 1. Coupling status of genetically engineered HEK293 cells.

(**A**) Dual whole cell patch clamp technique was used to measure transjunctional current (I_j) in response to indicated V_j in HEK293 cell pairs. Representative I_j recordings obtained from wildtype (WT), Cx45 knockout (Cx45KO), Cx43 knockout (Cx43KO), and double knockout with both Cx45 and Cx43 ablated (DKO) HEK293 cell pairs. (**B**) Bar graphs summarize the median percentage (the error bars indicate IQR) of coupled cell pairs (coupling%) in different HEK293 cells. Data points represent the number of transfections. (**C**) Bar graph illustrates the median coupling conductance (G_j) of HEK293 cell pairs. Data points represent the number of cell pairs. Kruskal–Wallis test followed by Dunn's *post hoc* test was used to compare different groups for all bar graphs. The statistical significance was indicated (**$P < 0.01$, and ***$P < 0.001$).

(Cx43KO) HEK293 cell pairs, but not in cell pair with both Cx43 and Cx45 knocked out (double knockout, DKO). The median percentage of recorded cell pairs showed GJ coupling (coupling%, Figure 1B) was calculated across several experiments for WT HEK293 (WT, 100 (88–100)%, $N = 6$), Cx45KO (100 (82–100)%, $N = 9$), Cx43KO (100 (96–100)%, $N = 6$), and DKO cell pairs (0 (0–0)%, $N = 10$). The coupling conductance (G_j) was calculated from each individual cell pair tested with median G_j, (4.9 (1.9–12.2) nS, $n = 20$) for WT, (2.4 (0.7–7.1) nS, $n = 38$) for Cx45KO, (0.7 (0.3–1.8) nS, $n = 29$) for Cx43KO, (0 (0–0) nS, $n = 39$) for DKO (Figure 1C). Both coupling% and G_j were significantly reduced for DKO cells compared with WT, Cx45KO, and Cx43KO cells (Figure 1).

V_j-gating properties of endogenous GJs in engineered HEK293 cells

To investigate V_j-gating properties of GJs in genetically engineered HEK293 cells, WT, Cx45KO, or Cx43KO cell pairs were selected for dual whole cell voltage clamp. I_js were recorded in response to a series of V_j pulses (±20 to ±100 mV). As shown in Figure 2, I_js of WT, Cx45KO, and Cx43KO, all showed mirror symmetrical V_j-dependent I_j deactivation. For GJs of WT and Cx45KO cells, the I_j deactivation was prominent when absolute V_j values were ≥60 mV, while the Cx43KO cells showed I_j deactivation when the absolute V_j values were ≥20 mV (Figure 2). To obtain V_j induced I_js with minimum V_j-gating for Cx43KO cells, we added an additional pair of V_j at ±5 mV, which indeed showed minimum V_j-dependent deactivation (Figure 2 gray colored V_js and I_js). The steady-state conductance was normalized to the initial peak conductance for each V_j pulse to obtain the normalized steady state conductance ($G_{j,ss}$). The $G_{j,ss}$ was then plotted against V_j for each of these engineered HEK293 cells as shown in Figure 2 right panels. The $G_{j,ss}$ – V_j plots could be fitted well with Boltzmann equations for both V_j-polarities for WT, Cx45KO, and Cx43KO cells (smooth lines in right panels of Figure 2 and Table 1 for Boltzmann parameters).
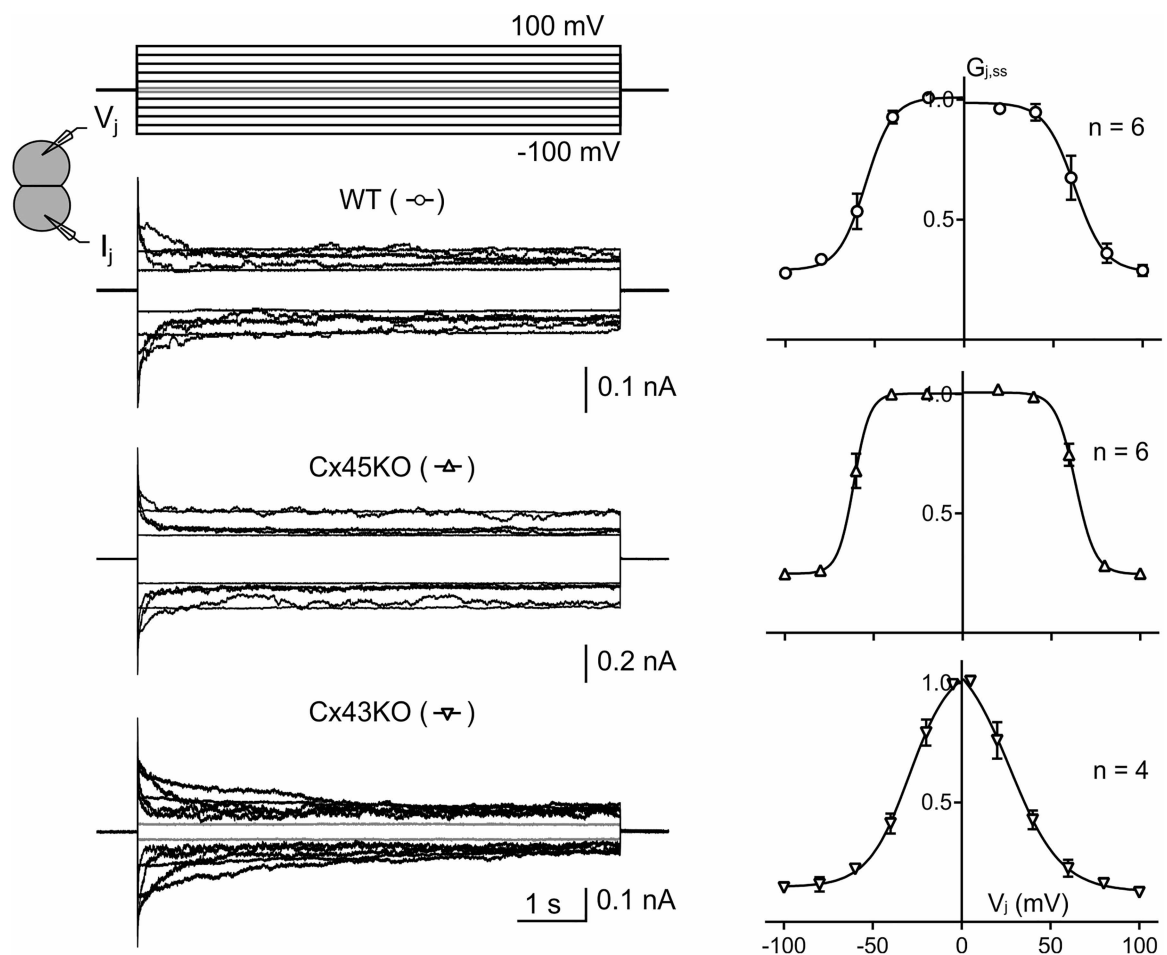
Figure 2. V$_j$-gating properties of genetic engineered HEK293 cells.
Superimposed transjunctional currents (I_js) in response to the indicated V_j pulses (±20 to ±100 mV, in the case of Cx43KO ±5 mV V_j pulses were also added and in gray color) for cell pairs of WT (open circles), Cx45KO (open triangles), and Cx43KO (open inverse triangles). Depending on the cells recorded, the absolute I_j amplitude values were either remained steady during the V_j pulse (at V_js of ±20 to ±40 mV for WT and Cx45KO cells and at V_j of ±5 mV for Cx43KO cells) or decreased mirror symmetrically during the V_j pulses (at the rest of the tested V_js). Normalized steady-state conductance ($G_{j,ss}$) was obtained and plotted against tested V_js (right panel). The $G_{j,ss}$ – V_j relationship could be fitted well by Boltzmann equations and the smooth lines in each plot represent Boltzmann fittings for both V_j polarities. The error bars represent the standard error of mean (±SEM). The number of cells pairs is indicated.

PORTLAND PRESS

Table 1. Boltzmann fitting parameters of functional homotypic and heterotypic gap junction channels

Cells	V_j polarity	G_{min}	V_0 (mV)[†]	A
WT ($n = 6$)	+	0.28 ± 0.05	62.0 ± 2.6	0.12 ± 0.04
	−	0.29 ± 0.03	55.2 ± 1.8	0.13 ± 0.03
Cx45KO ($n = 6$)	+	0.25 ± 0.02	$63.6 \pm 1.1^*$	0.18 ± 0.04
	−	0.25 ± 0.03	$61.3 \pm 1.2^{***}$	0.22 ± 0.15
Cx43KO ($n = 4$)	+	$0.13 \pm 0.03^*$	$27.2 \pm 4.0^{***}$	0.07 ± 0.015
	−	$0.15 \pm 0.02^*$	$29.4 \pm 2.3^{***}$	0.085 ± 0.014

Data in this table are the average ± SEM. Boltzmann parameters of WT, Cx45KO, and Cx43KO HEK293 cells are shown. Statistically significant differences are indicated (*$P < 0.05$; ***$P < 0.001$) versus the WT parameters at the respective V_j polarity; [†]the absolute values of V_0 are shown for each of the V_j polarities.

Unitary channel currents of engineered HEK293 cells

Cx45KO and Cx43KO HEK293 cell pairs sometimes showed only one functional GJ channel which allowed us to study single channel currents (i_js) at different V_js (Figure 3). All point histograms and Gaussian fits were used to measure the amplitudes of i_js for the main conducting state (the main open state) (Figure 3A, right panels). For Cx45KO cell pairs, one or more subconductance states (open arrows, also known as residue conductance states) as well as fully closed state (filled black arrows) were also observed in the recorded i_js (Figure 3A), while for Cx43KO cell pairs, only main open state could be identified. We constructed $i_j – V_j$ plot for Cx45KO and Cx43KO cell pairs (Figure 3B). Linear regressions for the $i_j – V_j$ plots were used to obtain the averaged slope single channel conductance for Cx45KO $\gamma_j = 107 \pm 1$ pS and for Cx43KO $\gamma_j = 38 \pm 1$ pS (Figure 3B).

Expression of several human connexins successfully formed functional GJs in double knockout HEK293 cells

To test if double knockout HEK293 cells (DKO) could be used to study recombinantly expressed human connexins, we transfected DKO cells with an expression vector containing human Cx45 (Cx45-IRES-GFP) and functional GJ channels were formed with V_j-gating profile nearly identical with those observed in Cx43KO HEK293 cells (Figure 4). While expressing the empty vector (only encoding reporter GFP) as a negative control resulted in no GJ coupling (Figure 4). Similarly, we were able to express several selected human connexins, Cx46, Cx50, Cx37, and Cx36, in the DKO cells which successfully formed homotypic GJs with their signature V_j-gating properties (Figure 4). Normalized steady-state junctional conductance ($G_{j,ss}$) was plotted against V_j (Figure 5). The $G_{j,ss} – V_j$ plots of cell pairs expressing Cx45 and Cx37 could be well fitted by Boltzmann equations (Figure 5 and Table 2). The Boltzmann parameters of these and our previously studied Cx46 and Cx50 GJs were very much similar to those obtained from the same connexins expressed in N2A cells, with the exception of the G_{min} of Cx37 GJ, which was consistently reduced for both positive and negative V_j polarities (Table 2). The exogenously expressed Cx45 GJ V_j-gating properties were also similar to those of endogenously expressed Cx45 (see Table 1 for Cx43KO). These data demonstrated that DKO HEK293 cells are an excellent model cell for patch clamp study of human GJs formed by these human connexins.

In poorly coupled DKO HEK293 cell pairs expressing Cx46 and Cx26, unitary channel currents (i_js) could be recorded, which is very useful in detailed mechanistic studies at a single GJ channel level with excellent signal noise ratio (Figure 6). The $i_j – V_j$ plot was constructed for each of these cell pairs and the slope single channel conductance (γ_j) for Cx46 (213 pS) and Cx26 (156 pS) was obtained (Figure 6).

Human congenital heart disease and arrhythmia linked Cx45 variant R184G failed to form morphological and functional GJs

To reveal the mechanism of a congenital heart disease and arrhythmia linked Cx45 variant R184G [45], we expressed this variant in DKO HEK293 cells in two expression vectors, i.e. GFP untagged Cx45 R184G-IRES-GFP and GFP tagged Cx45 R814G-GFP for functional and morphological studies respectively. As shown in Figure 7A,B, Cx45 R184G failed to form any functional GJ channels and were significantly different from cell pairs expressing WT Cx45 in both coupling% and coupling conductance (G_j). When GFP tagged WT Cx45 (Cx45-GFP) was expressed in DKO HEK293 cells, clusters of GJ plaques were identified at the cell-cell
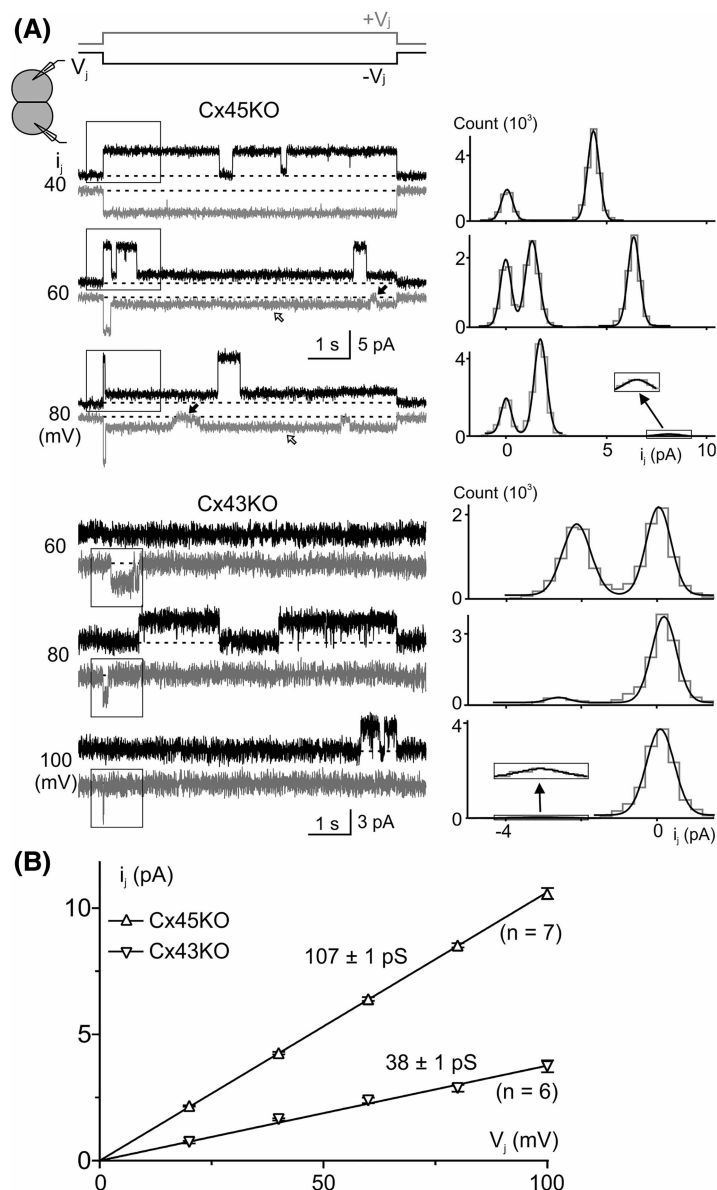
Figure 3. Single channel analysis of genetically engineered HEK293 cells.
(**A**) Single channel currents (i_js) recordings were shown in response to the indicated V_js ($-V_j$ in black and $+V_j$ in gray) from Cx45KO (top) and Cx43KO (bottom) cell pairs. The Cx45KO i_js showed subconductance state (or residue conductance state, open arrows) and fully closed state (filled arrows). All point histograms (gray) were constructed in the boxed regions on the original i_js shown on the left panels and Gaussian fitting curves (black smooth curves) were used to measure the amplitude of the i_js at the main open state. (**B**) The i_js from Cx45KO (open triangles) and Cx43KO (inverse open triangles) were plotted against V_js. Linear regressions were used to determine the slope single channel conductance (γ_j) for Cx45KO and Cx43KO cell pairs. The γ_js and the number of cell pairs are indicated.

junctions ([Figure 7C](#), arrows), whereas R184G-GFP failed to form any clusters of GJ plaque-like structures at the cell-cell interface ([Figure 7C](#)).

Discussion

In the present study we genetically engineered a commonly used human model cell line, HEK293 cells, to be connexin deficient by ablating the endogenous Cx43 and Cx45 (the double knockout or DKO HEK293 cells).
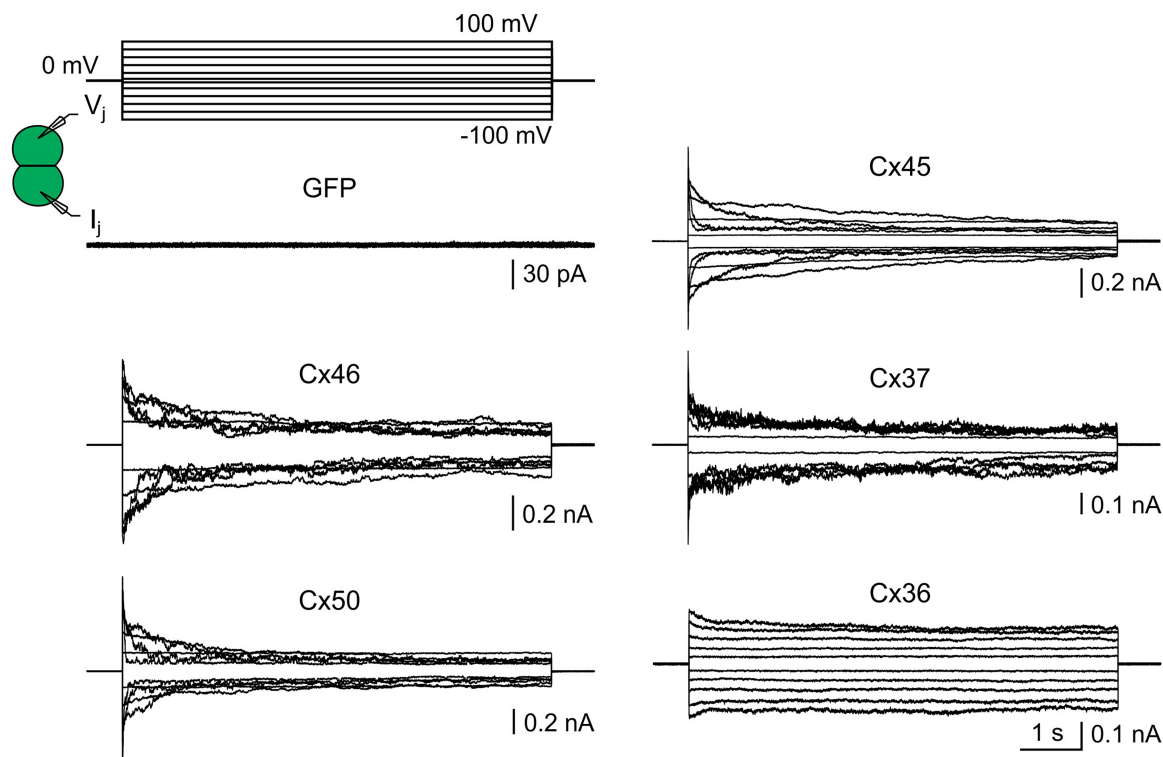
Figure 4. Expression of human connexins formed functional GJs in DKO HEK293 cells with signature V_j-gating properties.

Superimposed transjunctional currents (I_js) in response to the indicated V_j pulses (±20 to ±100 mV, in some cases also with ±5 mV) for DKO cell pairs expressing GFP, Cx46, Cx50, Cx45, Cx37, or Cx36 as indicated. Expression of GFP alone failed to form any functional GJ channels, while expression of Cx46, Cx50, Cx45, Cx37, or Cx36 formed functional GJs with their signature V_j-gating properties.

DKO HEK293 cells demonstrated excellent features for the functional study of GJs: (1) the DKO HEK 293 cells showed no GJ coupling ('clean' background) in multiple passages within the past few years; (2) expression of several exogenous human connexin genes individually, including Cx46, could successfully form functional GJs; (3) DKO HEK293 cells retained their accessibility for patch clamp analysis. Our dual patch clamp study on GJs formed by several human connexins (Cx46, Cx50, Cx45, Cx37, Cx36) demonstrated the feasibility of functional study of human GJs formed by these connexins, in the case of Cx46 and Cx26 it was possible to study at the single GJ channel level. Interestingly, the single Cx45 or Cx43 knock out HEK293 cells were found to be suitable for studying both macroscopic and single GJ channels on the endogenously expressed connexins. The genetically engineered HEK293 cells are excellent model cells to study human connexins either endogenously or exogenously expressed, including characterizing connexin variants linked to inherited diseases or those that exist in the general population [46]. A preliminary description of DKO HEK293 cells and successful application in studying human lens connexins was recently reported [47].

Mutations in more than 10 human connexin genes have been identified to possibly play a pathogenic role in inherited human diseases [7,8,48]. To ascertain whether these genetic variants play a pathogenic role in these diseases, one will need to have strong genetic evidence (e.g. co-segregation of disease with mutant carriers in multiple independent families), extremely low frequency or non-existence of the variant in the exomes of the general population (such as gnomAD) [49], and functional evidence of connexin mutants with altered function in either a cell model or an animal model [50]. For the functional studies on disease-linked connexin variants, each of the model systems showed some limitations as discussed below.

Mouse models of connexin variants are an excellent way to study human disease-linked variants and have been successful in recapitulating some aspects of the relevant human diseases [12,51,52]. The mouse models work especially well for those connexins that showed near identical protein sequences between mouse and
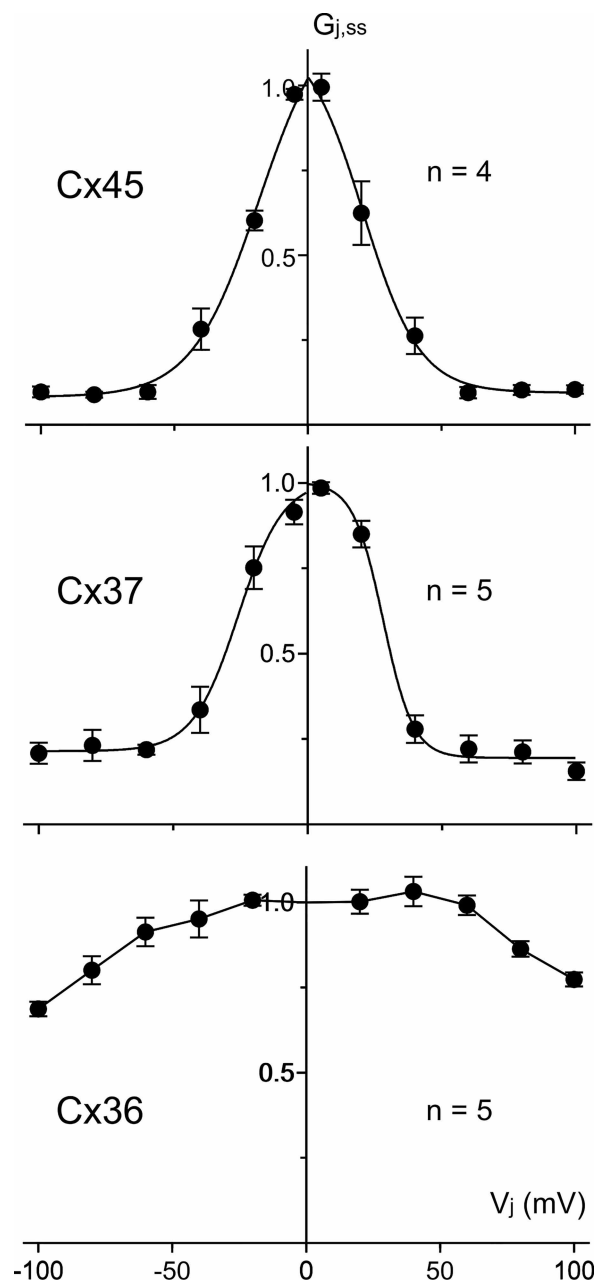
Figure 5. Normalized steady-state junctional conductance ($G_{j,ss}$) was plotted against V_j in cell pairs expressing Cx45, Cx37, and Cx36.

The $G_{j,ss} - V_j$ plots of both Cx45 and Cx37 could be well fitted by Boltzmann equations for each of their V_js, while in the case of Cx36 we were unable to fit the data with Boltzmann equations (the line was simply connecting the averaged data points). The number of cell pairs are indicated for each plot.

human connexins (such as Cx32 and Cx43 with 99% and 97% sequence identity, respectively). But in cases where connexins have lower sequence identity between human and mouse, e.g. Cx46 (71% sequence identity) and Cx31.1 (77% sequence identity), it is not clear if one should use mouse or human connexin as template to generate the variant mouse model or whether the resultant mouse model would recapitulate key pathological manifestations of the human connexin diseases. It is also important to note that the connexin tissue distribution in mice is not always the same as those in humans. For example, mouse heart atrio-ventricular (AV) nodal cells express both Cx45 and Cx30.2 while in the human heart AV nodal cells only Cx45 is expressed without

Table 2. Boltzmann fitting parameters of functional homotypic GJs expressed in DKO HEK293 cells

| GJs	V_j polarity	G_{min}	V_0 (mV)	A
Cx46 ($n = 5$)	+	0.10 ± 0.02	32 ± 1.7	0.18 ± 0.03
	−	0.16 ± 0.02	36.6 ± 2.1	0.21 ± 0.1
Cx50 ($n = 4$)	+	0.17 ± 0.02	35.5 ± 1.2	0.17 ± 0.04
	−	0.21 ± 0.02	37.5 ± 1.6	0.18 ± 0.07
Cx45 ($n = 4$)	+	0.08 ± 0.02	18.4 ± 3.7	0.08 ± 0.02
	−	0.09 ± 0.03	20.6 ± 3.6	0.09 ± 0.02
Cx37 ($n = 5$)	+	0.22 ± 0.03*	25.8 ± 2.5*	0.12 ± 0.03
	−	0.20 ± 0.02**	28.1 ± 1.5	0.18 ± 0.03

Data in this table are the average ± SEM. Boltzmann parameters of the indicated homotypic GJs are shown. Cx46 and Cx50 Boltzmann parameters are the same as reported previously [47]. Boltzmann parameters for Cx45 and Cx37 were compared with previous data [10,29] obtained for the same connexins expressed in N2A cells. Statistically significant differences are shown (*$P <$ 0.05; **$P < 0.001$) versus the same connexin at the indicated V_j polarity. V_0 are reported as absolute values. No data were shown for Cx36, as the $G_{j,ss} − V_j$ plot for Cx36 GJ could not be well fit by the Boltzmann equation.

any expression of the human Cx31.9 (the orthologue of mouse Cx30.2) [53–55]. In this case, the vulnerability of action potential propagation in the human heart AV nodal cells cannot be recapitulated in the mouse models [56]. In addition, relatively high costs and longer time required for developing mouse models for connexin mutants are some additional hindering factors to consider when using mouse models for newly discovered connexin variants. Thus, many laboratories choose to use *in vitro* cell models to study the functional outcome of human disease-linked connexin mutants.

As discussed earlier the commonly used cell models to study expressed human connexins showed some significant limitations, including non-mammalian expression system (*Xenopus* oocytes expression studies) with different post-translational modifications, non-human cell context (such as N2A or RIN cells) with different inter-species interactomes especially those connexins with more variabilities between human and rodent, and in those human model cells (such as HeLa and SKHep1) they tend to have a higher level of heterogeneous background coupling or some less favorable properties for functional studies using patch clamp [39]. Our genetically engineered HEK293 cells overcome some of these limitations. The DKO HEK293 cells have been successfully used to study not only the properties of homotypic GJs, but also heterotypic docking compatibilities of human lens connexins, Cx46, Cx50, and Cx43 [47]. Our present study extended the use of DKO HEK to several other human connexins, and they were all expressed well and formed functional GJs with different signature gating properties.

Among all the human disease linked connexin mutants, the most prevalent cases are mutations in Cx26 linked sensorineural hearing loss [57]. It is interesting to note that some Cx26 mutants are very severe and not only associated with hearing loss but also with skin diseases known as syndromic hearing loss [58]. Here we showed that Cx26 was able to form functional GJ channels in DKO HEK293 cells and in some cases with only one or two channels between a cell pair providing an excellent vehicle to study mechanistic defects associated Cx26 mutants in individual GJ channels. Expression of a congenital heart disease and arrhythmia linked mutation in Cx45 (R184G) in DKO HEK293 cells resulted in no functional GJ formed, similar to that observed in N2A cells [45]. The failure to cluster at the cell-cell junctions of Cx45 R184G in DKO HEK293 cells was also observed in HeLa cells (Chen and Bai unpublished observations). These functional and morphological studies demonstrate that DKO HEK293 cells are an excellent model to study disease-linked mutants. We believe that the GJ channel properties obtained from this human cell line would be a much better reflection of their function in the human body than those obtained from *Xenopus* oocyte and/or rodent cell line expression systems. We have summarized some key features of commonly used expression vehicles on their strengths and weaknesses for functional study of GJ channels (Table 3).

It is interesting to note that the single knockout of either Cx45 or Cx43 in HEK293 cells, yield a good level of endogenously expressed Cx43 or Cx45, respectively, for functional characterizations of GJs at both macroscopic and single GJ channel levels. This is a very convenient feature for studies on these human GJs, especially
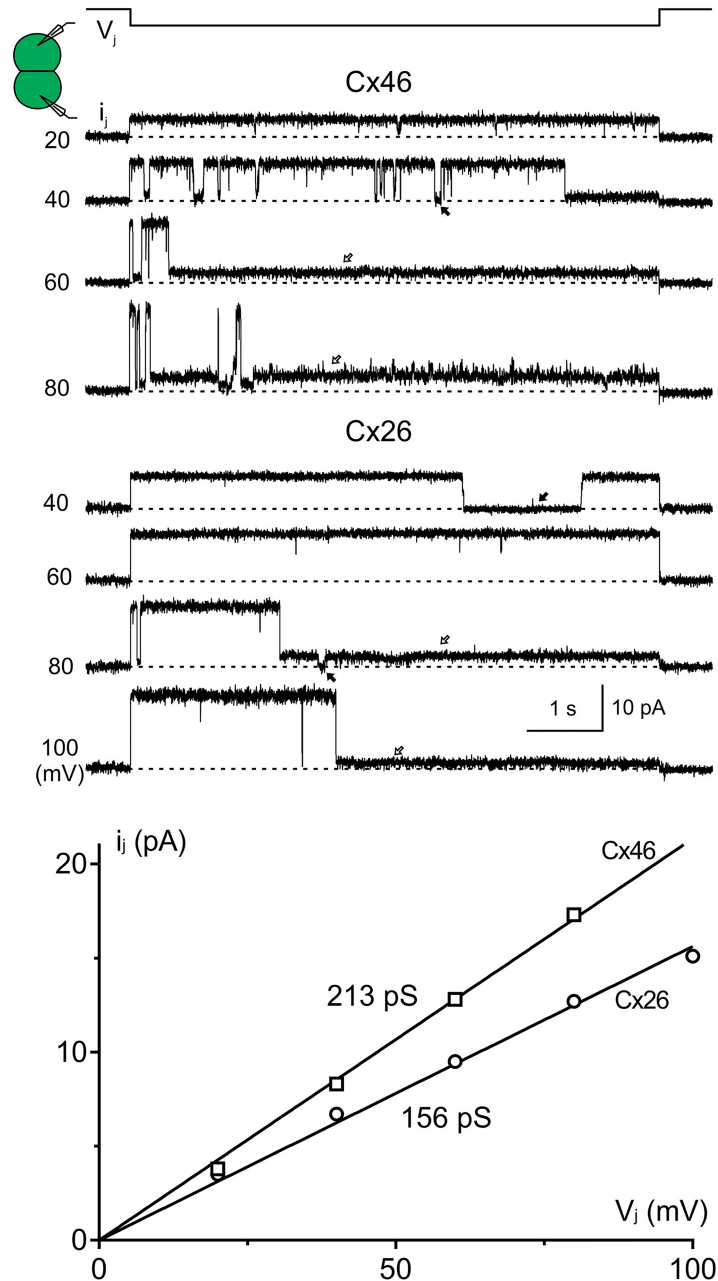
Figure 6. Single Cx46 and Cx26 GJ currents could be studied in DKO HEK293 cells.

Top panel shows the unitary transjunctional currents (i_js) recorded in response to the indicated V_j pulses in a DKO HEK293 cell pair expressing Cx46-IRES-GFP and Cx26-IRES-GFP. The amplitude of i_js increased with the increase of V_j in each case and the linear regression of the $i_j – V_j$ plot (bottom panel) for each of these cell pairs was used to obtain slope single channel conductance of Cx46 GJ (γ_j = 213 pS) and Cx26 GJ (γ_j = 156 pS). Open arrows on the i_js indicate residual conductance state, and the black filled arrow indicates fully closed state.

for Cx43 GJ which is extremely difficult to have optimized experimental conditions in recombinant overexpression model cells due to the following reasons. Depending on the connexins under study, the overexpression model cells tend to have a high level of expression of connexins because efficient promoters are commonly used in the expression cDNA vectors. Abundant connexin expression often ends up with highly GJ coupled cell pairs exceeding the ideal GJ coupling conductance range of under ~10 nS to have proper voltage clamp with minimum voltage clamp errors [59,60]. When the coupling conductance (G_j) is at ≥50 nS in a cell pair, then it
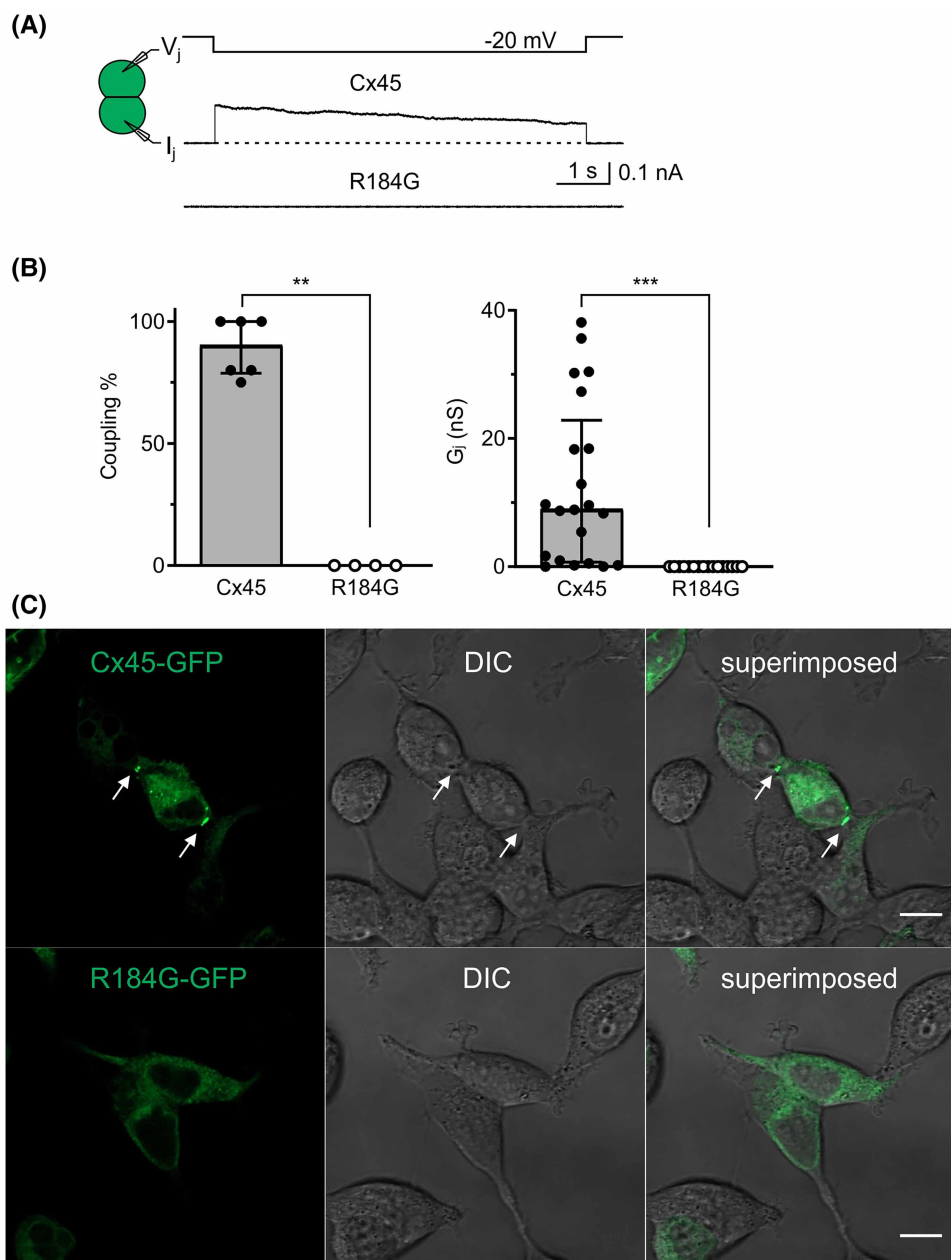
Figure 7. Cx45 R184G failed to form functional GJs in DKO HEK293 cells likely due to failed clustering at the cell-cell junctions.

(**A**) Dual whole cell patch clamp technique was used to measure transjunctional current (I_j) in response to indicated V_j in DKO HEK293 cell pairs. Representative I_j recordings obtained from cell pairs expressing untagged Cx45 or Cx45 R184G. (**B**) Bar graph on the left panel summarizes the median percentage (the error bars indicate IQR) of coupled cell pairs (coupling%) in cell pairs expressing Cx45 (filled circles) or Cx45 R184G (open circles). Data points represent the number of transfections. Bar graph on the right panel illustrates the median coupling conductance (G_j) of cell pairs expressing Cx45 and Cx45 R184G. Data points represent the number of cell pairs. Mann–Whitney test was used to compare different groups for these bar graphs. The statistical significance was indicated (**$P < 0.01$, and ***$P < 0.001$). (**C**) Confocal images of DKO HEK293 cells expressing GFP tagged Cx45 (Cx45-GFP) or Cx45-R184G (R184G-GFP). GJ plaque like clusters of Cx45-GFP could be observed at the cell-cell junctions, whereas R184G-GFP failed to form any clusters at the cell-cell junctions. Fluorescence, differential interference contrast (DIC), and superimposed images are shown as indicated. These are representative images from three independent experiments. Scale bar = 10 μm.

Table 3. Comparison of model cells used for functional study of GJ channels

Model cells	Mammalian cells	Human cell context[§]	Coupling conductance measurements	Single channel recordings[‡]	Background GJ coupling[†]
Xenopus oocyte pairs	No	No	Yes	No	High
N2A cells	Yes	No	Yes	Yes	None or extremely low
HeLa cells	Yes	Yes	Yes	Yes	Moderate
RIN cells	Yes	No	Yes	Yes	Low
DKO HEK293 cells	Yes	Yes	Yes	Yes	None or extremely low

Notes: DKO HEK293, double knockout human embryonic kidney 293; [§]some human connexins, like Cx46, does not express well in N2A cell, but human Cx46 expressed well in DKO HEK293 cells; [‡]it is possible to perform single GJ channel current recording for some connexins; [†]several factors could affect the background GJ coupling depending on the model cells, consistency of culture conditions, genetic stability of the model cells, etc. Built-in positive and negative controls should be routinely included to ensure the data obtained are not due to background GJs.

is impossible to know for sure if the cell pair is highly GJ coupled or simply an apparent 'cell pair' not yet finished cell proliferation into two cells (known as cytoplasmic bridges, i.e. the apparent two cells in the 'cell pair' is still connected by their cytoplasm) which we encounter from time to time especially when studying recombinantly expressed Cx43. The data on these apparently highly GJ coupled cell pairs cannot be counted as GJ coupled pairs and must be discarded from our experimental data. To reduce the probability of having apparently highly GJ coupled cell pairs, we often design our experiments to capture the early phase of connexin expression by reducing the replating time, finding cell pairs with low and different levels of fluorescent reporters between the two cells in a pair (when using in frame fusion tagged or bicistronic expression vectors with GFP or RFP as reporter), which worked well in some experiments but not without negative consequences, such as reducing replating time could artificially increase the rate of false negative cell pairs (lowering the percentage of coupled cell pairs in our bar graphs for connexins fully capable to form GJs) and often technically very challenging as we can only patch on cells fully attached to the glass coverslips (usually require 30 min or longer). Different connexins appear to have somewhat different abilities in forming GJs between cell pairs and Cx43 is one of the easiest and earliest to form functional GJs and therefore the hardest to obtain optimized G_j in cell pairs and virtually impossible to study single channel properties without introduction of GJ blockers or use acidifications as described in some earlier studies for Cx43 GJs or other connexin GJs [61,62]. While in the Cx45KO or Cx43KO HEK293 cells, we could find cell pairs with G_j under 10 nS routinely and was feasible to obtain cell pairs with only 1–2 functional GJ channels with excellent signal noise ratio to perform single channel analysis without any introduction of GJ blockers. This is critical if one would like to study mechanisms of certain chemical modulations for these two cardiovascular GJ channels.

Genetically engineered HEK293 cells in our hand showed excellent genetic stability. The DKO HEK293 cells consistently show no GJ coupling over the last few years with multiple passages [47] and the single Cx43KO and Cx45KO also showed consistent GJ channel properties as those previously reported for Cx45 and Cx43 GJs [34,63]. We believe that these features of genetically engineered HEK293 cells are much better than those of HeLa or SKHep1 cells and will be used widely for characterizing human GJ channel properties using patch clamp and may also serve as a convenient model cell for dye-transfer studies and structural studies on recombinantly expressed human GJs.

In conclusion, we genetically engineered human HEK293 cells to either completely or partially delete the endogenously expressed Cx43 and Cx45. These cells showed excellent features for patch clamp analysis of human GJs and studying human disease-linked connexin variants in a human cell context will facilitate more accurate identification for pathogenicity of more and more identified disease-linked connexin variants.

Materials and methods
CRISPR-Cas9 gene ablation

A version of HEK293 cells were purchased from Agilent (known as AD-293 cells with catalog part# 240085). CRISPR-Cas9 was used to genetically ablate Cx43 as described [47,64]. Briefly, HEK293 cells were transiently

transfected using Mirus TransIT-LT1 transfection reagent (MIR 2300, Mirus Bio, Madison, WI, U.S.A.) with the pSpCas9(BB)-2A-GFP plasmid (PX458, Addgene, Cambridge, MA, U.S.A.), which encodes for the Cas9 protein and a cloning background for the single guide RNA (sgRNA). The gRNAs used to target the exon of *GJA1* (human Cx43) were designed using the Sanger CRISPR finder (https://wge.stemcell.sanger.ac.uk/find_crisprs), and predicted to have low off-targets: 5′ ATGGGTGACTGGAGCGCCTT 3′ (Figure 8A). Following transfection, GFP-expressing cells were sorted using fluorescence activated cell sorting system at London Regional Flow Cytometry Facility and individual clones were examined for Cx43 ablation using Western blot (Figure 8C) and dual patch clamp method. Following similar procedures, Cx45 was also ablated on Cx43 knockout line as well as wildtype (WT) HEK293 cells with the following sgRNAs 5′ ACAACCATTCC ACATTTGTG 3′ (Figure 8B). As no reliable antibody for Cx45 could be identified in our hands, we used dual patch clamp method to screen for successful knockout lines.

Cell culture

WT, Cx43 knockout (Cx43KO), Cx45 knockout (Cx45KO), and double knockout (DKO with both Cx43 and Cx45 knockout) HEK293 cells were cultured in DMEM containing 4.5 g/l D-(+)-glucose, 584 mg/l L-glutamine (4 mM), 110 mg/l sodium pyruvate, 10% fetal bovine serum (FBS), 1% penicillin (100 units/ml), and 1% streptomycin (100 μg/ml or 172 μM), in an incubator with 5% CO_2 at 37°C similar to those described earlier [65,66]. Prior to patch clamp recording, HEK293 cells were replated onto glass coverslips for different durations. For study on coupling percentage (coupling%) of cell pairs and coupling conductance (G_j) of WT and Cx45KO the replating time was 0.7–1.5 h. For Cx43KO cells, a much longer replating time (18–20 h) was used to obtain data for coupling% and G_j. For DKO cells both 0.7–1.5 and 18–20 h replating time were used. To increase the odds of observing single GJ channel current (i_js) in cell pairs, we shorten the replating time to 0.5–1 h for Cx45KO and Cx43KO HEK293 cells.

Expression vectors and transfection

Human Cx46, Cx50, Cx45, and Cx37 were subcloned individually into a pIRES2-EGFP expression vector as described in our earlier studies [29,30,47]. Human Cx36 cDNA was obtained from R&D Systems (Cat# RDC1280) and was subcloned into pIRES2-EGFP expression vector between restriction enzyme sites NheI and EcoRI. All these human connexins were sequenced to ensure no errors in these expression vectors.

DKO HEK293 cells were transfected at a 1:2 ratio of cDNA : transfection reagent, with 0.6–1 μg of a cDNA construct and 1.2–2 μl of X-tremeGENE HP DNA transfection reagent (Roche Diagnostics GmbH, Cat#06366546001) in Opti-MEM + GlutaMAX-I medium (Cat#51985-034) for 5 h. Medium was changed back to FBS-containing DMEM after transfection until the following day, where transfected DKO HEK293 cells were replated onto glass coverslips. Coverslips were transferred to a recording chamber after 2–3 h, where isolated cell pairs successfully transfected with the connexins of interest together with the GFP as reporter were selected to study the formation of various homotypic GJs in our DKO HEK293 cells via dual whole cell patch clamp.

Western blot

Soluble proteins were separated via SDS–PAGE and transferred to a 0.45 μm nitrocellulose membrane. The following primary antibodies were used for immunoblotting: rabbit anti Cx43 (C6219, Sigma–Aldrich); mouse anti GAPDH (MAB374, Chemicon). The following secondary antibodies were used: goat anti-rabbit IRDye 800 (611-132-122, Rockland) and goat anti-mouse Alexa Fluor 680 (A21076, ThermoFisher). The relative quantities of the immunoblotted proteins were normalized to GAPDH using the Odyssey Infrared Imaging System (Li-Cor Biosciences, Lincoln, NE, U.S.A.). As shown in Figure 8C, Cx43 was successfully deleted.

Electrophysiological recording

Glass coverslips with HEK293 cells were placed into a recording chamber on an upright fluorescent microscope (BX51WI, Olympus). The chamber was filled with extracellular solution (ECS) at room temperature (21–24°C). The ECS contained (in mM): 135 NaCl, 2 CsCl, 2 $CaCl_2$, 1 $MgCl_2$, 1 $BaCl_2$, 10 HEPES, 5 KCl, 5 D-(+)-glucose, 2 sodium pyruvate, pH 7.4 with 1 M NaOH, and with an osmolarity of 310–320 mOsm. Patch pipettes were pulled using a micropipette puller (PC-100, Narishige International USA Inc., Amityville, NY, U.S.A.) and filled with intracellular solution containing (in mM): 130 CsCl, 10 EGTA, 0.5 $CaCl_2$, 2 Na_2ATP, 3 MgATP, 10 HEPES, adjusted to pH 7.2 with 1 M CsOH, and with an osmolarity of 290–300 mOsm. Patch pipette resistance was in the range of 2–4 MΩ. Isolated HEK293 cell pairs were selected for dual whole cell voltage clamp
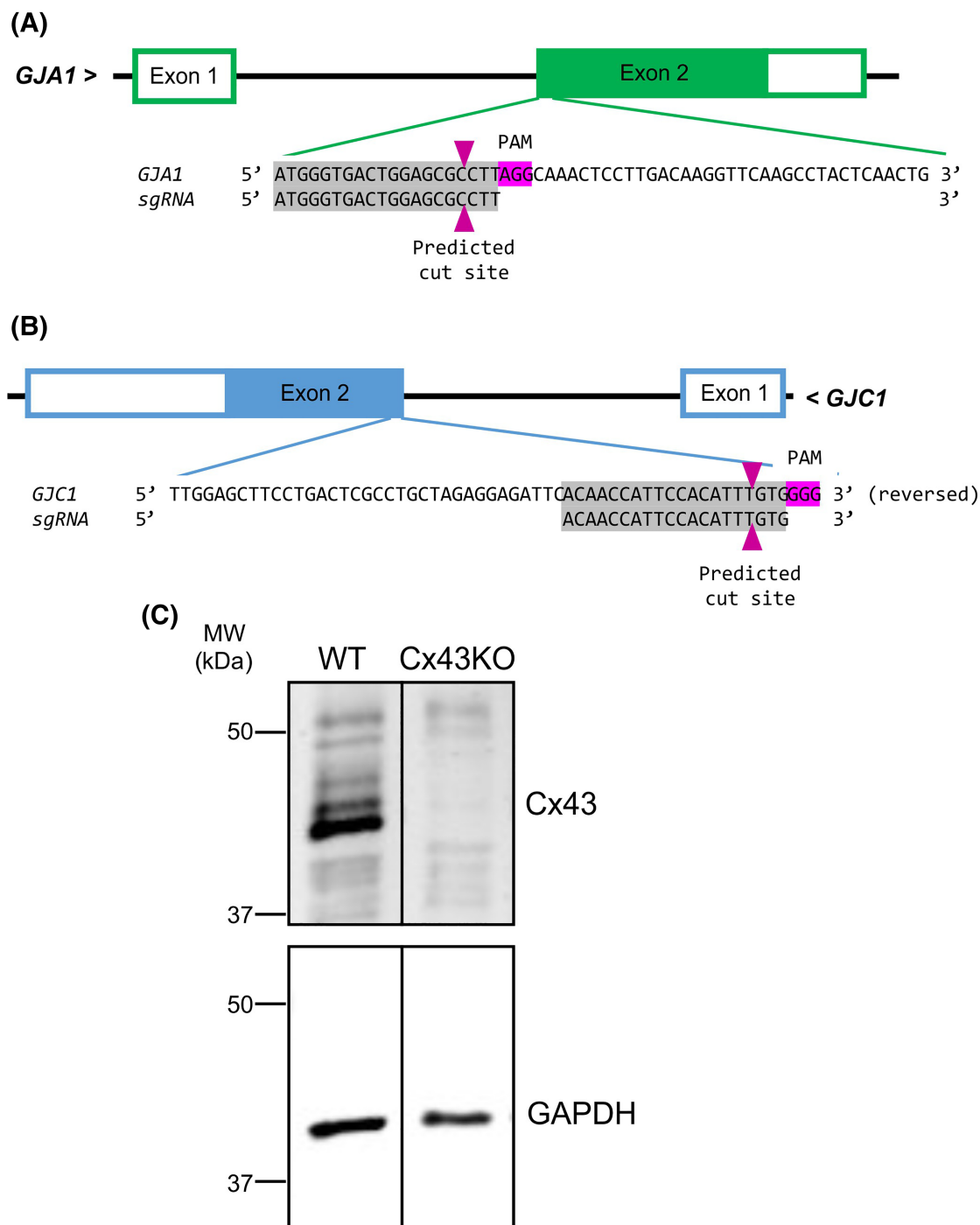
Figure 8. Design of sgRNA to knockout *GJA1* (encoding Cx43) and *GJC1* (encoding Cx45) genes in HEK293 cells.
(**A**) and (**B**) panels illustrate the gene structure of *GJA1* and *GJC1* and the designed single guide RNA (sgRNA) targeting at the beginning of the coding regions (filled green and blue bars) of these genes. (**C**) Western blot shows that Cx43 is expressed and showed typical multiple bands in wildtype (WT) HEK293 cells. CRISPR-Cas9 gene ablation targeting the *GJA1* gene (encoding Cx43) was successful in deleting Cx43 (Cx43KO) in this clone of HEK293 cells. GAPDH was used as a loading control.

experiment. Initially, both cells in a pair were voltage clamped at 0 mV, then one cell in the pair was stepped to a 20 mV voltage pulse of 7 s (pulsing cell) while the other cell of the pair was holding at a constant voltage of 0 mV (current recording cell). Transjunctional currents (I_js) were amplified with a MultiClamp 700A amplifier

(Molecular Devices, Sunnyvale, CA, U.S.A.). I_js were low-pass filtered at 1 kHz (Bessel filter) and digitized via an AD/DA converter at a sampling frequency of 10 kHz (Digidata 1550, Molecular Devices) to a computer with pClamp 10.7 (Molecular Devices).

Transjunctional voltage-dependent gating

To study transjunctional voltage dependent gating (V_j-gating) properties in GJ coupled cell pairs, a series of voltage pulses (±20 to ±100 mV with 20 mV increment) were administrated to one of the cell pair to establish transjunctional voltage (V_j). The other cell was held at 0 mV to record transjunctional current (I_j). In experiments with Cx43KO HEK293 cells and recombinant expression of some human connexins, V_j pulses of ±5 mV were also used because some GJs exhibited V_j-gating at ±20 mV. In most cases, I_j peaked at the beginning of a 7-s V_j pulse, then declines to a steady state at the end (more pronounced with high V_js). The GJ coupling conductance (G_j) was calculated by $G_j = I_j/V_j$ at V_js of ±20 mV for each engineered or WT HEK293 cell pair. Cell pairs that have G_j >50 nS were excluded from coupling% analysis because it is impossible to differentiate the GJ-coupled cell pairs from 'the apparently highly coupled cell pairs (due to cytoplasmic bridge)'. Only cell pairs that have G_j lower than 9 nS were selected for V_j-gating study to avoid voltage clamp errors [59,60]. The steady-state G_j was normalized to the peak G_j to obtain a normalized steady-state junctional conductance ($G_{j,ss}$) for each V_j. A $G_{j,ss}$ - V_j plot was then generated and fitted with a two-state Boltzmann equation for each V_j polarity. The Boltzmann equation is:

$$G_{j,ss} = \frac{G_{max} - G_{min}}{1 + \exp[A(V_j - V_0)]} + G_{min}$$

V_0 is the V_j at which the normalized steady-state conductance, $G_{j,ss} = [(G_{max} - G_{min})/2 + G_{min}]$. G_{max} is the normalized maximum conductance, while G_{min} is the normalized minimum conductance. 'A' is the slope of the fitted curve that represents the V_j-gating sensitivity [67].

Single GJ channel current recording and analysis

Single channel currents (i_js) were observed in cell pairs with few active GJ channels. The recorded i_js were further filtered using a low-pass Gaussian filter at 200 Hz in Clampfit for measuring current amplitude and display in figures. The amplitude of i_j values for the fully open state at different V_j values were measured with fitting Gaussian functions on all point current amplitude histograms. The i_js of different cell pairs were averaged under the same V_j regardless of V_j polarity to generate i_j – V_j plot. Linear regression of i_j – V_j plot was used to obtain slope unitary conductance (γ_j) as described earlier [66,68].

Localization of Cx45 variant R184G

Fluorescent protein GFP was inframe fusion tagged at the carboxyl terminus of Cx45 variant R184G (R184G-GFP) similar to earlier studies [10,30]. R184G-GFP and WT Cx45-GFP were expressed individually in DKO HEK293 cells. Culture and transfection were the same as described earlier for functional studies. One day after transfection, cells were replated on glass bottom dises for 3–5 h to allow formation of morphological GJ plaques. Confocal microscope (Zeiss LSM800 with Airyscan, Zeiss, Oberkochen, Germany) with 40× water-immersion lens (NA1.2) was used to study the localization of Cx45-GFP and R184G-GFP. Bright green fluorescent clusters (deemed to be GJ plaques) could be observed at the cell-cell junctions of Cx45-GFP expressing cells, but no morphological GJ plaques were observed at cell-cell junctions in R184G-GFP expressing cells.

Statistical analysis

The data on percentage of cell pairs coupled (coupling%) and coupling conductance (G_j) bar graphs are expressed as median values and the error bars represent interquartile range (IQR). Kruskal–Wallis followed by Dunn's *post hoc* test was used to compare coupling% and G_j. For analysis of V_j-gatings of the Boltzmann fitting parameters for Cx43KO and Cx45KO HEK293 cells and i_j – V_j plots, data are expressed as mean ± SEM. An unpaired Student's *t*-test was used to compare Boltzmann parameters and single channel conductance (γ_j). Statistical significance is indicated with the asterisks on the graphs (*$P < 0.05$; **$P < 0.01$; or ***$P < 0.001$).

Data Availability

All data in this study are available from the corresponding author upon request.

Competing Interests

The authors declare that there are no competing interests associated with the manuscript.

Funding

CRediT Author Contribution

Donglin Bai: Conceptualization, Resources, Supervision, Visualization, Project administration, Writing — review and editing. **Honghong Chen**: Conceptualization, Resources, Data curation, Formal analysis, Investigation, Visualization, Methodology, Writing — original draft. **Yi x. Li**: Data curation, Formal analysis, Investigation, Visualization, Methodology, Writing — review and editing. **Robert S. Wong**: Resources, Data curation, Formal analysis, Investigation, Visualization, Methodology, Writing — review and editing. **Jessica L. Esseltine**: Conceptualization, Resources, Data curation, Formal analysis, Supervision, Investigation, Visualization, Methodology, Writing — review and editing.

Acknowledgements

Abbreviations

Cx43, connexin43; Cx45, connexin45; Cx50, connexin50; ECS, extracellular solution; FBS, fetal bovine serum; GJ, gap junction; $G_{j,ss}$, normalized steady-state junctional conductance; G_j, gap junctional conductance; HEK, human embryonic kidney; IQR, interquartile range; I_j, macroscopic junctional current; i_j, single channel current; KO, knockout; RIN, rat insulinoma; sgRNA, single guide RNA; V_j, transjunctional voltage; WT, wildtype.

References

1   Saez, J.C., Berthoud, V.M., Branes, M.C., Martinez, A.D. and Beyer, E.C. (2003) Plasma membrane channels formed by connexins: their regulation and functions. *Physiol. Rev.* **83**, 1359–1400 https://doi.org/10.1152/physrev.00007.2003

2   Goodenough, D.A. and Paul, D.L. (2009) Gap junctions. *Cold Spring Harb. Perspect. Biol.* **1**, a002576 https://doi.org/10.1101/cshperspect.a002576

3   Söhl, G. and Willecke, K. (2004) Gap junctions and the connexin protein family. *Cardiovasc. Res.* **62**, 228–232 https://doi.org/10.1016/j.cardiores.2003.11.013

4   Lucaciu, S.A., Leighton, S.E., Hauser, A., Yee, R. and Laird, D.W. (2023) Diversity in connexin biology. *J. Biol. Chem.* **299**, 105263 https://doi.org/10.1016/j.jbc.2023.105263

5   Laird, D.W. (2006) Life cycle of connexins in health and disease. *Biochem. J.* **394**, 527–543 https://doi.org/10.1042/BJ20051922

6   Laird, D.W. and Lampe, P.D. (2022) Cellular mechanisms of connexin-based inherited diseases. *Trends Cell Biol.* **32**, 58–69 https://doi.org/10.1016/j.tcb.2021.07.007

7   Laird, D.W., Naus, C.C. and Lampe, P.D. (2017) Snapshot: connexins and disease. *Cell* **170**, 1260–1260.e1261 https://doi.org/10.1016/j.cell.2017.08.034

8   Srinivas, M., Verselis, V.K. and White, T.W. (2018) Human diseases associated with connexin mutations. *Biochim. Biophys. Acta* **1860**, 192–201 https://doi.org/10.1016/j.bbamem.2017.04.024

9   Tong, J.J., Khan, U., Haddad, B.G., Minogue, P.J., Beyer, E.C., Berthoud, V.M. et al. (2021) Molecular mechanisms underlying enhanced hemichannel function of a cataract-associated Cx50 mutant. *Biophys. J.* **120**, 5644–5656 https://doi.org/10.1016/j.bpj.2021.11.004

10 Li, T., Chen, H., Li, X., Stathopulos, P.B. and Bai, D. (2023) Inherited disease-linked arginine76/75 mutants in Cx50 and Cx45 showed impaired homotypic and heterotypic gap junction function, but not Cx43. *Biochem. J.* **480**, 1051–1077 https://doi.org/10.1042/BCJ20230081

11 Abrams, C.K., Peinado, A., Mahmoud, R., Bocarsly, M., Zhang, H., Chang, P. et al. (2018) Alterations at Arg(76) of human connexin 46, a residue associated with cataract formation, cause loss of gap junction formation but preserve hemichannel function. *Am. J. Physiol. Cell Physiol.* **315**, C623–C635 https://doi.org/10.1152/ajpcell.00157.2018

12 Dobrowolski, R., Sasse, P., Schrickel, J.W., Watkins, M., Kim, J.S., Rackauskas, M. et al. (2008) The conditional connexin43G138R mouse mutant represents a new model of hereditary oculodentodigital dysplasia in humans. *Hum. Mol. Genet.* **17**, 539–554 https://doi.org/10.1093/hmg/ddm329

13 Sanchez, H.A., Slavi, N., Srinivas, M. and Verselis, V.K. (2016) Syndromic deafness mutations at Asn 14 differentially alter the open stability of Cx26 hemichannels. *J. Gen. Physiol.* **148**, 25–42 https://doi.org/10.1085/jgp.201611585

14 Santa Cruz, A., Mese, G., Valiuniene, L., Brink, P.R., White, T.W. and Valiunas, V. (2015) Altered conductance and permeability of Cx40 mutations associated with atrial fibrillation. *J. Gen. Physiol.* **146**, 387–398 https://doi.org/10.1085/jgp.201511475

15 White, T.W., Wang, H., Mui, R., Litteral, J. and Brink, P.R. (2004) Cloning and functional expression of invertebrate connexins from Halocynthia pyriformis. *FEBS Lett.* **577**, 42–48 https://doi.org/10.1016/j.febslet.2004.09.071

16 Barrio, L.C., Suchyna, T., Bargiello, T., Xu, L.X., Roginski, R.S., Bennett, M.V. et al. (1991) Gap junctions formed by connexins 26 and 32 alone and in combination are differently affected by applied voltage. *Proc. Natl Acad. Sci. U.S.A.* **88**, 8410–8414 https://doi.org/10.1073/pnas.88.19.8410

17 Verselis, V.K., Ginter, C.S. and Bargiello, T.A. (1994) Opposite voltage gating polarities of two closely related connexins. *Nature* **368**, 348–351 https://doi.org/10.1038/368348a0

18 Skerrett, I.M., Merritt, M., Zhou, L., Zhu, H., Cao, F., Smith, J.F. et al. (2001) Applying the Xenopus oocyte expression system to the analysis of gap junction proteins. *Methods Mol. Biol.* **154**, 225–249 https://doi.org/10.1385/1-59259-043-8:225

19 Shui, Y. and Wang, Z.-W. (2022) Recording gap junction current from Xenopus oocytes. *JoVE* **179**, e63361 https://doi.org/10.3791/63361

20 García, I.E. Villanelo, F., Contreras, G.F., Pupo, A., Pinto, B.I., Contreras, J.E. et al. (2018) The syndromic deafness mutation G12R impairs fast and slow gating in Cx26 hemichannels. *J. Gen. Physiol.* **150**, 697–711 https://doi.org/10.1085/jgp.201711782

21 Maton, G., Lorca, T., Girault, J.A., Ozon, R. and Jessus, C. (2005) Differential regulation of Cdc2 and Aurora-A in Xenopus oocytes: a crucial role of phosphatase 2A. *J. Cell Sci.* **118**, 2485–2494 https://doi.org/10.1242/jcs.02370

22 Dehennaut, V., Slomianny, M.C., Page, A., Vercoutter-Edouart, A.S., Jessus, C., Michalski, J.C. et al. (2008) Identification of structural and functional O-linked N-acetylglucosamine-bearing proteins in Xenopus laevis oocyte. *Mol. Cell. Proteomics* **7**, 2229–2245 https://doi.org/10.1074/mcp.M700494-MCP200

23 Malik, M.Q., Bertke, M.M. and Huber, P.W. (2014) Small ubiquitin-like modifier (SUMO)-mediated repression of the Xenopus oocyte 5 S rRNA genes. *J. Biol. Chem.* **289**, 35468–35481 https://doi.org/10.1074/jbc.M114.609123

24 Ebihara, L., Beyer, E.C., Swenson, K.I., Paul, D.L. and Goodenough, D.A. (1989) Cloning and expression of a Xenopus embryonic gap junction protein. *Science* **243**, 1194–1195 https://doi.org/10.1126/science.2466337

25 Srinivas, M., Costa, M., Gao, Y., Fort, A., Fishman, G.I. and Spray, D.C. (1999) Voltage dependence of macroscopic and unitary currents of gap junction channels formed by mouse connexin50 expressed in rat neuroblastoma cells. *J. Physiol.* **517**, 673–689 https://doi.org/10.1111/j.1469-7793.1999.0673s.x

26 Olmsted, J.B., Carlson, K., Klebe, R., Ruddle, F. and Rosenbaum, J. (1970) Isolation of microtubule protein from cultured mouse neuroblastoma cells. *Proc. Natl Acad. Sci. U.S.A.* **65**, 129–136 https://doi.org/10.1073/pnas.65.1.129

27 Xin, L., Gong, X.Q. and Bai, D. (2010) The role of amino terminus of mouse Cx50 in determining transjunctional voltage-dependent gating and unitary conductance. *Biophys. J.* **99**, 2077–2086 https://doi.org/10.1016/j.bpj.2010.07.032

28 Jassim, A., Aoyama, H., Ye, W.G., Chen, H. and Bai, D. (2016) Engineered Cx40 variants increased docking and function of heterotypic Cx40/Cx43 gap junction channels. *J. Mol. Cell. Cardiol.* **90**, 11–20 https://doi.org/10.1016/j.yjmcc.2015.11.026

29 Kim, N.K., Santos-Miranda, A., Chen, H., Aoyama, H. and Bai, D. (2019) Heterotypic docking compatibility of human connexin37 with other vascular connexins. *J. Mol. Cell. Cardiol.* **127**, 194–203 https://doi.org/10.1016/j.yjmcc.2018.12.013

30 Ye, W.G., Yue, B., Aoyama, H., Kim, N.K., Cameron, J.A., Chen, H. et al. (2017) Junctional delay, frequency, and direction-dependent uncoupling of human heterotypic Cx45/Cx43 gap junction channels. *J. Mol. Cell. Cardiol.* **111**, 17–26 https://doi.org/10.1016/j.yjmcc.2017.07.117

31 Hopperstad, M.G., Srinivas, M. and Spray, D.C. (2000) Properties of gap junction channels formed by Cx46 alone and in combination with Cx50. *Biophys. J.* **79**, 1954–1966 https://doi.org/10.1016/S0006-3495(00)76444-7

32 Tong, J.J., Sohn, B.C., Lam, A., Walters, D.E., Vertel, B.M. and Ebihara, L. (2013) Properties of two cataract-associated mutations located in the NH2 terminus of connexin 46. *Am. J. Physiol. Cell Physiol.* **304**, C823–C832 https://doi.org/10.1152/ajpcell.00344.2012

33 Rubinos, C., Villone, K., Mhaske, P.V., White, T.W. and Srinivas, M. (2014) Functional effects of Cx50 mutations associated with congenital cataracts. *Am. J. Physiol. Cell Physiol.* **306**, C212–C220 https://doi.org/10.1152/ajpcell.00098.2013

34 Bukauskas, F.F., Angele, A.B., Verselis, V.K. and Bennett, M.V. (2002) Coupling asymmetry of heterotypic connexin 45/ connexin 43-EGFP gap junctions: properties of fast and slow gating mechanisms. *Proc. Natl Acad. Sci. U.S.A.* **99**, 7113–7118 https://doi.org/10.1073/pnas.032062099

35 Contreras, J.E., Saez, J.C., Bukauskas, F.F. and Bennett, M.V. (2003) Gating and regulation of connexin 43 (Cx43) hemichannels. *Proc. Natl Acad. Sci. U.S.A.* **100**, 11388–11393 https://doi.org/10.1073/pnas.1434298100

36 Yum, S.W., Zhang, J.X., Valiunas, V., Kanaporis, G., Brink, P.R., White, T.W. et al. (2007) Human connexin26 and connexin30 form functional heteromeric and heterotypic channels. *Am. J. Physiol. Cell Physiol.* **293**, C1032–C1048 https://doi.org/10.1152/ajpcell.00011.2007

37 Yum, S.W., Zhang, J. and Scherer, S.S. (2010) Dominant connexin26 mutants associated with human hearing loss have trans-dominant effects on connexin30. *Neurobiol. Dis.* **38**, 226–236 https://doi.org/10.1016/j.nbd.2010.01.010

38 Frattini, A., Fabbri, M., Valli, R., De Paoli, E., Montalbano, G., Gribaldo, L. et al. (2015) High variability of genomic instability and gene expression profiling in different HeLa clones. *Sci. Rep.* **5**, 15377 https://doi.org/10.1038/srep15377

39 Magnotti, L.M., Goodenough, D.A. and Paul, D.L. (2011) Functional heterotypic interactions between astrocyte and oligodendrocyte connexins. *Glia* **59**, 26–34 https://doi.org/10.1002/glia.21073

40 Eghbali, B., Kessler, J.A. and Spray, D.C. (1990) Expression of gap junction channels in communication-incompetent cells after stable transfection with cDNA encoding connexin 32. *Proc. Natl Acad. Sci. U.S.A.* **87**, 1328–1331 https://doi.org/10.1073/pnas.87.4.1328

41 Moreno, A.P., Eghbali, B. and Spray, D.C. (1991) Connexin32 gap junction channels in stably transfected cells: unitary conductance. *Biophys. J.* **60**, 1254–1266 https://doi.org/10.1016/S0006-3495(91)82159-2

42 Burt, J.M., Nelson, T.K., Simon, A.M. and Fang, J.S. (2008) Connexin 37 profoundly slows cell cycle progression in rat insulinoma cells. *Am. J. Physiol. Cell Physiol.* **295**, C1103–C1112 https://doi.org/10.1152/ajpcell.299.2008

43 Cottrell, G.T., Wu, Y. and Burt, J.M. (2002) Cx40 and Cx43 expression ratio influences heteromeric/ heterotypic gap junction channel properties. *Am. J. Physiol. Cell Physiol.* **282**, C1469–C1482 https://doi.org/10.1152/ajpcell.00484.2001

44 Ek Vitorín, J.F., Pontifex, T.K. and Burt, J.M. (2016) Determinants of Cx43 channel gating and permeation: the amino terminus. *Biophys. J.* **110**, 127–140 https://doi.org/10.1016/j.bpj.2015.10.054

45 Li, Y.J., Wang, J., Ye, W.G., Liu, X.Y., Li, L., Qiu, X.B. et al. (2023) Discovery of GJC1 (Cx45) as a new gene underlying congenital heart disease and arrhythmias. *Biology (Basel)* **12**, 346 https://doi.org/10.3390/biology12030346

46 Bai, D., Wang, J., Li, T., Chan, R., Atalla, M., Chen, R.C. et al. (2021) Differential domain distribution of gnomAD- and disease-linked connexin missense variants. *Int. J. Mol. Sci.* **22**, 7832 https://doi.org/10.3390/ijms22157832

47 Wong, R.S., Chen, H., Li, Y.X., Esseltine, J.L., Stathopulos, P.B. and Bai, D. (2024) Human Cx50 Isoleucine177 prevents heterotypic docking and formation of functional gap junction channels with Cx43. *Am. J. Physiol. Cell Physiol.* **326**, C414–C428 https://doi.org/10.1152/ajpcell.00634.2023

48   Amberger, J.S., Bocchini, C.A., Scott, A.F. and Hamosh, A. (2019) OMIM.org: leveraging knowledge across phenotype-gene relationships. *Nucleic Acids Res.* **47**, D1038–D1043 https://doi.org/10.1093/nar/gky1151

49   Karczewski, K.J., Francioli, L.C., Tiao, G., Cummings, B.B., Alföldi, J., Wang, Q. et al. (2020) The mutational constraint spectrum quantified from variation in 141,456 humans. *Nature* **581**, 434–443 https://doi.org/10.1038/s41586-020-2308-7

50   Oza, A.M., DiStefano, M.T., Hemphill, S.E., Cushman, B.J., Grant, A.R., Siegert, R.K. et al. (2018) Expert specification of the ACMG/AMP variant interpretation guidelines for genetic hearing loss. *Hum. Mutat.* **39**, 1593–1613 https://doi.org/10.1002/humu.23630

51   Lubkemeier, I., Bosen, F., Kim, J.S., Sasse, P., Malan, D., Fleischmann, B.K. et al. (2015) Human Connexin43E42K mutation from a sudden infant death victim leads to impaired ventricular activation and neonatal death in mice. *Circ. Cardiovasc. Genet.* **8**, 21–29 https://doi.org/10.1161/CIRCGENETICS.114.000793

52   Sargiannidou, I., Vavlitou, N., Aristodemou, S., Hadjisavvas, A., Kyriacou, K., Scherer, S.S. et al. (2009) Connexin32 mutations cause loss of function in Schwann cells and oligodendrocytes leading to PNS and CNS myelination defects. *J. Neurosci.* **29**, 4736–4749 https://doi.org/10.1523/JNEUROSCI.0325-09.2009

53   Bukauskas, F.F., Kreuzberg, M.M., Rackauskas, M., Bukauskiene, A., Bennett, M.V., Verselis, V.K. et al. (2006) Properties of mouse connexin 30.2 and human connexin 31.9 hemichannels: implications for atrioventricular conduction in the heart. *Proc. Natl Acad. Sci. U.S.A.* **103**, 9726–9731 https://doi.org/10.1073/pnas.0603372103

54   Kreuzberg, M.M., Willecke, K. and Bukauskas, F.F. (2006) Connexin-mediated cardiac impulse propagation: connexin 30.2 slows atrioventricular conduction in mouse heart. *Trends Cardiovasc. Med.* **16**, 266–272 https://doi.org/10.1016/j.tcm.2006.05.002

55   Frank, M., Wirth, A., Andrie, R.P., Kreuzberg, M.M., Dobrowolski, R., Seifert, G. et al. (2012) Connexin45 provides optimal atrioventricular nodal conduction in the adult mouse heart. *Circ. Res.* **111**, 1528–1538 https://doi.org/10.1161/CIRCRESAHA.112.270561

56   Seki, A., Ishikawa, T., Daumy, X., Mishima, H., Barc, J., Sasaki, R. et al. (2017) Progressive atrial conduction defects associated with bone malformation caused by a connexin-45 mutation. *J. Am. Coll. Cardiol.* **70**, 358–370 https://doi.org/10.1016/j.jacc.2017.05.039

57   Chan, D.K. and Chang, K.W. (2014) GJB2-associated hearing loss: systematic review of worldwide prevalence, genotype, and auditory phenotype. *Laryngoscope* **124**, E34–E53 https://doi.org/10.1002/lary.24332

58   Lee, J.R. and White, T.W. (2009) Connexin-26 mutations in deafness and skin disease. *Expert Rev. Mol. Med.* **11**, e35 https://doi.org/10.1017/S1462399409001276

59   Wilders, R. and Jongsma, H.J. (1992) Limitations of the dual voltage clamp method in assaying conductance and kinetics of gap junction channels. *Biophys. J.* **63**, 942–953 https://doi.org/10.1016/S0006-3495(92)81664-8

60   Bai, D. and Cameron, J.A. (2016) Patch clamp analysis of gap junction channel properties. In *Gap Junction Channels and Hemichannels* (Bai, D. and Saez, J.C., eds), pp. 93–114, CRC Press, Boca Raton, FL

61   Bai, D., del Corsso, C., Srinivas, M. and Spray, D.C. (2006) Block of specific gap junction channel subtypes by 2-aminoethoxydiphenyl borate (2-APB). *J. Pharmacol. Exp. Ther.* **319**, 1452–1458 https://doi.org/10.1124/jpet.106.112045

62   Burt, J.M. and Spray, D.C. (1988) Single-channel events and gating behavior of the cardiac gap junction channel. *Proc. Natl Acad. Sci. U.S.A.* **85**, 3431–3434 https://doi.org/10.1073/pnas.85.10.3431

63   Bukauskas, F.F., Bukauskiene, A., Bennett, M.V. and Verselis, V.K. (2001) Gating properties of gap junction channels assembled from connexin43 and connexin43 fused with green fluorescent protein. *Biophys. J.* **81**, 137–152 https://doi.org/10.1016/S0006-3495(01)75687-1

64   Esseltine, J.L., Brooks, C.R., Edwards, N.A., Subasri, M., Sampson, J., Séguin, C. et al. (2020) Dynamic regulation of connexins in stem cell pluripotency. *Stem Cells* **38**, 52–66 https://doi.org/10.1002/stem.3092

65   Sun, Y., Yang, Y.Q., Gong, X.Q., Wang, X.H., Li, R.G., Tan, H.W. et al. (2013) Novel germline GJA5/connexin40 mutations associated with lone atrial fibrillation impair gap junctional intercellular communication. *Hum. Mutat.* **34**, 603–609 https://doi.org/10.1002/humu.22278

66   Yue, B., Haddad, B.G., Khan, U., Chen, H., Atalla, M., Zhang, Z. et al. (2021) Connexin 46 and connexin 50 gap junction channel properties are shaped by structural and dynamic features of their N-terminal domains. *J. Physiol.* **599**, 3313–3335 https://doi.org/10.1113/JP281339

67   Spray, D.C., Harris, A.L. and Bennett, M.V. (1981) Equilibrium properties of a voltage-dependent junctional conductance. *J. Gen. Physiol.* **77**, 77–93 https://doi.org/10.1085/jgp.77.1.77

68   Tejada, M.G., Sudhakar, S., Kim, N.K., Aoyama, H., Shilton, B.H. and Bai, D. (2018) Variants with increased negative electrostatic potential in the Cx50 gap junction pore increased unitary channel conductance and magnesium modulation. *Biochem. J.* **475**, 3315–3330 https://doi.org/10.1042/BCJ20180523